Journal of Alloys and Compounds 615 (2014) 761–764

Contents lists available at ScienceDirect

Journal of Alloys and Compounds

journal homepage: www.elsevier.com/locate/jalcom

Magnetic and structural transitions in $CaMn_{0.96}Mo_{0.04}O_3$

E.V. Mostovshchikova *, R.I. Zainullina, N.G. Bebenin, T.I. Arbuzova, N.I. Solin, S.V. Naumov

Institute of Metal Physics, Ural Division of RAS, 620990 Ekaterinburg, Russia

ARTICLE INFO

Article history:
Received 11 April 2014
Received in revised form 18 June 2014
Accepted 27 June 2014
Available online 5 July 2014

Keywords:
Electron-doped manganite
$CaMn_{1-x}Mo_xO_3$
Magnetic transition
Structural transition
Elastic properties

ABSTRACT

The magnetic, transport and elastic properties of $CaMn_{0.96}Mo_{0.04}O_3$ polycrystal are reported. The magnetic data of the paramagnetic region point to the magnetic polarons. The transition from the paramagnetic state into the antiferromagnetic state of G-type occurs near 93 K, the crystal orthorhombic structure being unchanged. The transition from the paramagnetic orthorhombic phase into the C-type antiferromagnetic monoclinic phase is revealed at about 130–140 K, the transition taking place in small regions of the sample.

1. Introduction

Rare earth manganites $Re_{1-x}A_xMnO_3$ (where *Re* is rare earth element, *A* is alkaline earth one Sr, Ca or Ba) are attractive due to strong interaction between structural, magnetic, and charge subsystems. The colossal magnetoresistance observed in the hole-doped manganites is one of manifestations of this interaction (see, for example, reviews [1–4]). After investigations of the Mn^{3+}-rich $Re_{1-x}A_xMnO_3$ ($x < 0.5$) the scientists turned to studying the properties of Mn^{4+}-rich (electron doped) manganites with $x > 0.5$.

The parent $CaMnO_3$ manganite has orthorhombic *Pnma* structure with Mn^{4+} ion being located in the centre of the oxygen octahedron. $CaMnO_3$ is antiferromagnet of G-type in which Mn^{4+} spin is antiparallel to the spins of six nearest neighbor Mn^{4+} ions; Neel temperature T_N^G is about 110–130 K depending on the concentration of oxygen vacancies [5].

In $CaMnO_3$, the electron configuration of Mn^{4+} ion is $t_{2g}^3e_g^0$. The t_{2g} electrons are localized and completely spin-polarized; the e_g states are empty. The orbitals near the Fermi level E_F are Mn $t_{2g}\uparrow$ orbitals with a spin up (with small admixture of O *2p*). Above E_F, Mn $e_g\uparrow$ and Mn $t_{2g}\downarrow$ bands are located; the bands formed by Mn $e_g\downarrow$ orbitals are still higher and the states of Ca ions lie well below E_F.

The Mn^{3+} ions can be created in $CaMnO_3$ by doping with *Re* ions. In such a case, Mn–O distances and Mn–O–Mn angles are changed due to difference in ionic radii of Ca and *Re* ions and Jahn–Teller effect, so that MnO_6 octahedrons are deformed. If Mn^{3+} content is equal or higher than 0.1 some part of the sample undergoes transition from orthorhombic to monoclinic structure with charge/orbital ordering. At 150–200 K in this part of the crystal with monoclinic structure the magnetic transition from paramagnetic into the C-state occurs [6]. Other part of the manganites remains orthorhombic and undergoes the magnetic transition from paramagnetic to G-state at about 100–120 K. Therefore below 100–120 K, there are the nonuniform magnetic and structural states: the monoclinic C-phase and orthorhombic G-phase coexist.

Another way for creating Mn^{3+} ions is the oxygen deficient in $CaMnO_{3-\delta}$. At $\delta = 0.25$ the number of Mn^{4+} and Mn^{3+} ions is equal. In such nonstoichiometric $CaMnO_{3-\delta}$ the resistivity decreases as a result of the appearance of additional charge carriers [7–9] excepting for some δ when the ordering of the oxygen vacancies occurs producing strong localization of the charge carriers and high resistivity. In $CaMnO_{3-\delta}$ the transition into C-state was not observed for any δ.

The electron doping of $CaMnO_3$-based manganites can also be done by substitution of pentavalent (Nb^{5+}, Ta^{5+}, V^{5+}, etc.) or hexavalent (W^{6+}, Mo^{6+}) ions for Mn^{4+} [10–17]. In contrast to Ca-site doping, when the magnetic state of the manganite is changed only as the result of lattice deformation and strong interrelation between spin and charge subsystems, the Mn-site doping has direct influence on spin subsystem because just Mn-ions have localized t_{2g} electrons which form magnetic moment.

The Mn-site doping results in the decrease of the resistivity and appearance of the C-state [13] as Ca-site doping does. Therefore one may expect the appearance of C-state with monoclinic

* Corresponding author.
E-mail address: mostovsikova@imp.uran.ru (E.V. Mostovshchikova).

http://dx.doi.org/10.1016/j.jallcom.2014.06.179
0925-8388/

structure and charge/orbital ordering in $CaMn_{1-x}Me_xO_3$ near $x = 0.10$ if *Me* is a pentavalent ion and near $x = 0.05$ in the case when *Me* is hexavalent ion. However, the phase diagram of $CaMn_{1-x}Mo_xO_3$ obtained by the neutron powder diffraction and magnetic susceptibility and reported in [13] shows the C-state only when x is higher than 0.06. Perhaps, it takes place because the valence of Mo-ions is lower than 6+. Another source of this discrepancy may be small volume of the C monoclinic phase but the data published so far are insufficient to choose between these alternatives.

We have studied the magnetic, transport and elastic properties of the $CaMn_{0.96}Mo_{0.04}O_3$ polycrystal. The measurement of the sound velocity and the internal friction is known to be extremely sensitive method for detecting structural phase transitions. The comparison of the magnetic and transport data together with the elastic ones lets to make a conclusion about the phases in $CaMn_{0.96}Mo_{0.04}O_3$.

2. Samples and experimental methods

The $CaMn_{0.96}Mo_{0.04}O_3$ polycrystal was prepared by solid state reaction from stoichiometric CaO, MnO_2 and MoO_3. The synthesis was carried out in the following stages: the first step was annealing during 50 h at $T = 790$–900 °C with intermediate grindings, then there was the annealing during 8 h at 900–1150 °C, final annealing of pressed pellets during 8 h was performed at 1375 °C. The $CaMn_{0.96}Mo_{0.04}O_3$ polycrystal is single-phase. At room temperature, the crystal structure is orthorhombic with the parameters $a = 5.291$ Å, $b = 7.483$ Å ($b/\sqrt{2}$=5.292 A), $c = 5.293$ Å, $v = 52.40$ Å^3, which are close to those reported in [13].

The temperature (T) and magnetic field (H) dependences of magnetization σ were measured by SQUID (Quantum design) magnetometer in the Magnetometry Center of the Institute of Metal Physics. Magnetic data were recorded after cooling in magnetic field of 50 kOe (field cooling, FC) and after cooling without applied magnetic field (zero field cooling, ZFC). The $\sigma(T)$ dependence was measured in the magnetic field of 50 kOe in the temperature range of 5–300 K at heating (after ZFC) and cooling (FC regime). The magnetization curves $\sigma(H)$ were measured at $T = 5$ K in the magnetic field up to 50 kOe. The *ac* magnetic susceptibility $\chi_{ac}(T)$ were recorded by SQUID at heating and cooling in the range of 5–300 K with the excitating field $H_{ac} = 4$ Oe for frequency $f = 100$ Hz. Also in the temperature range of 120–610 K, the susceptibility $\chi = \sigma/H$ was measured by Faraday balance. The measurements were carried out in the field of 1.76 kOe at $T < 295$ K and at $H = 4.45$ kOe at $295 < T < 610$ K.

The resistivity ρ was measured in zero magnetic field and in the magnetic field $H = 7$ kOe by four probe technique at heating regime with the rate 2–3 K/min after ZFC. Magnetoresistance (MR) was calculated as $\Delta\rho/\rho_0 = [\rho(H) - \rho(0)]/\rho(0)$.

Longitudinal sound velocity V_l and internal friction Q^{-1} were determined by the composite oscillator method [18]. The resonance frequency and quality of the mechanical system consisting of a sample and a quartz rod exciting longitudinal vibrations were measured and then V_l and Q^{-1} were calculated for the sample. The frequency was of the order of 100 kHz. The measurements were carried out in a helium gas atmosphere under heating and cooling with a rate of about 20 K per hour. The length of the polycrystalline sample was 30 mm.

3. Experimental results

Fig. 1 shows the temperature dependence of the magnetization $\sigma(T)$ measured in the magnetic field of 50 kOe at heating after ZFC. At $T = 5$ K, the magnetization is equal to 17 emu/g. The derivative $d\sigma/dT$ has minimum at $T = 93$ K. No thermal hysteresis was observed. Inset in Fig. 1 shows the $\sigma(H)$ dependence measured at $T = 5$ K. The $\sigma(H)$ dependence is almost linear, $\sigma(H = 0)$ is slightly greater than 5 emu/g. Saturation of magnetization was not achieved in the fields used in our experiment.

Fig. 2 shows the real part of *ac* magnetic susceptibility vs. temperature taken at heating (after ZFC). One can see the narrow peak at $T = 93$ K i.e. at the temperature at which the extremum in $d\sigma/dT$ takes place. In the inset in Fig. 2 the inverse paramagnetic susceptibility, $1/\chi$, is plotted against temperature. The curve is almost linear when temperature exceeds 260 K; at lower T, the experimental points lie below the straight line. The high-temperature susceptibility follows the Curie–Weiss law $\chi = C/(T - \theta)$, where C is the Curie–Weiss constant $C = N\mu_{eff}^2/3k_B$. The linear fitting of $\chi^{-1}(T)$ curve in the range of 260 K < T < 610 K gives $\theta \approx 0$ and effective magnetic moment $\mu_{eff} = 4.99\ \mu_B$, which is significantly higher than theoretical value $\mu_{eff} = 3.96\ \mu_B$ calculated in assumption of non-interactive magnetic moments of Mn^{4+} and Mn^{3+} ions.

In Fig. 3 the temperature dependence of the resistivity is presented. The $\rho(T)$ behavior is semiconductor-like with $d\rho/dT < 0$ except for the range from 260 to 280 K where $d\rho/dT$ is positive but very small in value. The deep minimum at $T = 102$ K and weak peculiarity around $T = 137$ K are detected on the curve $d\rho/dT$ as function of T (Inset in Fig. 3).

Magnetoresistance determined for $H = 7$ kOe is presented in Inset in Fig. 3. Magnetic field decreases the resistivity, so that magnetoresistance is negative. One can see some peculiarities at the $\Delta\rho(T)/\rho_0$ curve: deep minimum at $T = 102$ K and minimum at $T = 136$ K. It is worth noting that the peculiarities in the $\Delta\rho(T)/\rho_0$ curve are located at the same temperatures as the peculiarities in the $d\rho(T)/dT$ curve.

Fig. 4 shows temperature dependence of the sound velocity $V_l(T)$ measured at heating (solid symbols) and cooling (open symbols). When the T is higher than 135 K the temperature hysteresis is observed. The $V_l(T)$ plots have a bell shaped form with maximum ~6160 m/s at around 250–300 K. The sound velocity of $CaMn_{0.96}Mo_{0.04}O_3$ is significantly higher than that in hole-doped La-manganites (see, for example, [19,20]) but is somewhat lower than value of V_l in undoped $CaMnO_3$ [21]. One can see steps on the $V_l(T)$ curves (in temperature range of 136–140 K at heating and in the range of 133–143 K at cooling). There are also other

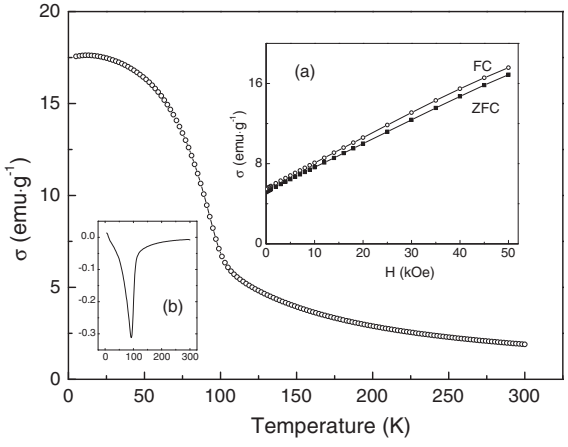

Fig. 1. The temperature dependence of magnetization measured at 50 kOe in heating regime after ZFC. Inset (a) the magnetization vs. magnetic field at $T = 5$ K after ZFC (solid symbols) and FC (open symbols) and inset (b) $d\sigma/dT$ as a function of T.

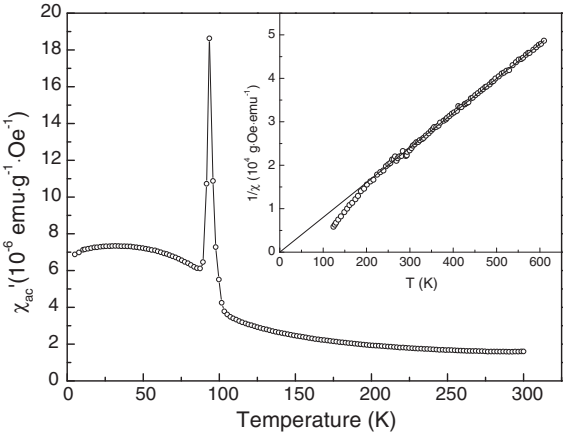

Fig. 2. χ'_{ac} against T measured at heating (after ZFC). Inset the inverse paramagnetic susceptibility $1/\chi$ vs. T. The straight line is linear fitting.

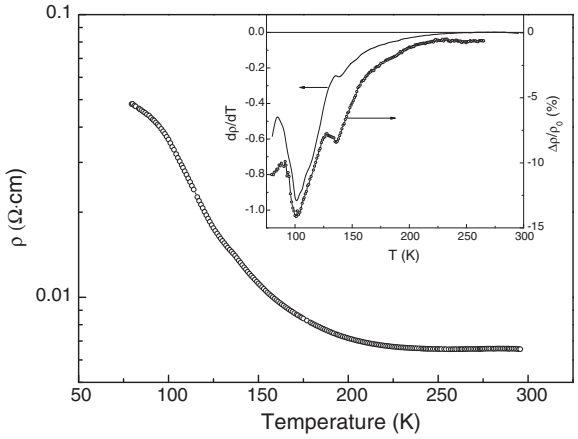

Fig. 3. The resistivity, measured at $H = 0$ at heating (after ZFC), vs. temperature. Inset: $d\rho/dT$ (left axis) and $\Delta\rho/\rho_0$ (right axis) as functions of temperature.

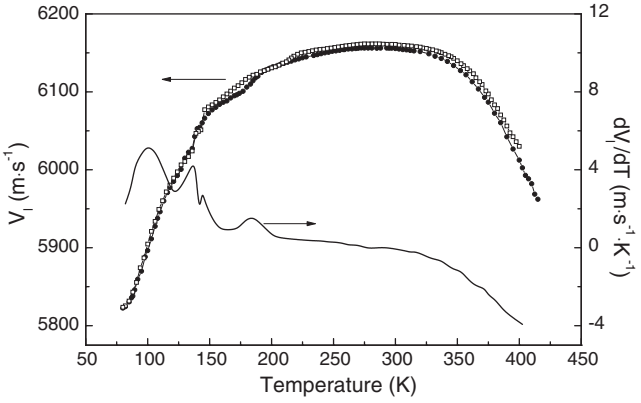

Fig. 4. The temperature dependences of the sound velocity (left axis) and dV_l/dT at heating (right axis). Solid symbols correspond to heating, open symbols correspond to cooling.

peculiarities in dV_l/dT curves: at heating one sees maxima at 100 and 185 K, at cooling (not shown) the maxima are at 96, 177 and 214 K.

Fig. 5 shows the temperature dependences of the internal friction taken at heating and cooling. The $Q^{-1}(T)$ curve measured at heating has three peaks situated at 106, 133, and 185 K. The curve taken at cooling has four maxima that are at 109, 141, 170, and 214 K. We see that the peculiarity temperatures in the $Q^{-1}(T)$ curves are close to those in $V_l(T)$.

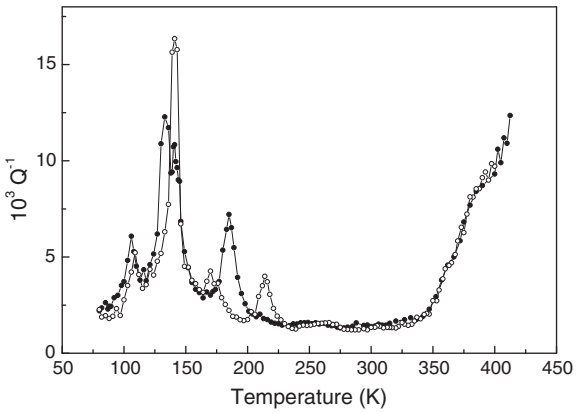

Fig. 5. The temperature dependences of the internal friction measured at heating (solid symbols) and cooling (open symbols).

4. Discussion

The pronounced extrema in $d\sigma/dT$ and the peak in χ'_{ac} at $T = 93$ K together with linear dependence of $\sigma(H)$ and small non-zero spontaneous magnetization at $T = 5$ K indicate that the transition from the paramagnetic state to G state with weak ferromagnetism occurs at $T_N^G = 93$ K. This statement agrees with results of other works [11,12,22].

In the paramagnetic state, the high value of effective magnetic moment $\mu_{eff} = 4.99\ \mu_B$ estimated from the curve $\chi^{-1}(T)$ in the temperature range $360 < T < 610$ K indicates the magnetic polarons to exist. In the frame of Varma model [23] the effective magnetic moment is given by

$$\mu_{eff}^2 = [y(S_1 + PS_2)(S_1 + PS_2 + 1) + (1 - y - Py)S_2(S_2 + 1)]g^2\mu_B^2. \quad (1)$$

Here $0 \leqslant P \leqslant 6$ is the number of polarized spins of Mn^{4+} which are nearest to Mn^{3+} ion, $S_1 = 2$ is the spin of Mn^{3+} ion, $S_2 = 3/2$ is the spin of Mn^{4+} ion, $(S_1 + PS_2)$ is polaron's spin, y is the concentration of Mn^{3+} ions, μ_B is Bohr magneton, g-factor can be taken to be equal 2. The composition of our manganite can be written as $Ca^{2+}(Mn^{4+}_{0.917}Mn^{3+}_{0.083})_{0.96}Mo^{6+}_{0.04}O_3$. As the concentration of Mn^{3+} is $y = 0.083$, the effective magnetic moment is $4.58\mu_B$ if the number of polarized Mn^{4+} spins is $P = 2$, when $P = 3$, the effective moment is $\mu_{eff} = 5.08\ \mu_B$. Since near a given Mn^{3+} there are 6 nearest Mn^{4+} (or 5 if Mo^{6+} occupies a nearest Mn position) we may infer that the mean spin of Mn^{4+} involved in the magnetic polaron state is lower than 3/2.

The transition from the paramagnetic state to the G-state manifests itself not only in magnetic properties but also in kinetic and elastic ones, which is evident from the extrema in $d\rho/dT$, $\Delta\rho/\rho_0$, dV_l/dT, and Q^{-1} observed near 100 K. Such behavior near the transition temperature is typical of antiferromagnets.

In the range of 130–140 K, clear extrema in $d\rho/dT$, $\Delta\rho/\rho_0$, Q^{-1} and the steps in $V_l(T)$ curve are observed while the temperature dependences of magnetization and magnetic susceptibility have no peculiarities. In addition, the thermal hysteresis in $V_l(T)$ and $Q^{-1}(T)$ is observed above ≈130 K. This indicates that in the interval from approximately 130 to 140 K there occurs a phase transition at which both crystal structure and magnetic state change. Remembering that the electron doping of $CaMnO_3$ can result in the transition from the paramagnetic state with orthorhombic structure into the C antiferromagnetic state with monoclinic structure we may infer that the peculiarities are due to such transition.

At first glance, our finding contradicts the neutron data of [13] because in that work, the monoclinic C-phase in $CaMn_{1-x}Mo_xO_3$ was reported only for $x > 0.06$ while in our manganite the molybdenum content is 0.04. To solve the contradiction one has to take into account that the sound velocity and internal friction are extremely sensitive to small change in crystal structure. Therefore our results simply indicate that the phase transition into the monoclinic C-phase occurs in a very small part of our $CaMn_{0.96}Mo_{0.04}O_3$ manganite. Unfortunately, our data are insufficient for determining the volume of the monoclinic C-phase.

It is to be noted that in the range of 170–214 K some peculiarities in $dV_l(T)/dT$ and $Q^{-1}(T)$ curves are observed. Their origin remains unclear.

5. Summary

The magnetic, transport and elastic properties of $CaMn_{0.96}Mo_{0.04}O_3$ are studied in wide temperature range. In the paramagnetic state ($260 < T < 610$ K), the magnetic polarons are shown to exist. At lower temperatures, there are at least two phase transitions. The first one is

the transition from the paramagnetic state into the antiferromagnetic state of G-type near 93 K, the crystal orthorhombic structure being unchanged. Another transition is the transition from the paramagnetic orthorhombic phase into the C-type antiferromagnetic monoclinic phase at about 130–140 K. The latter transition occurs in small regions of the $CaMn_{0.96}Mo_{0.04}O_3$ manganite.

Acknowledgments

This work was supported by the Program of fundamental research of Russian Academy of Sciences "Quantum mesoscopic and disordered structures" (project 12-P-2-1034) and Russian Foundation for Basic Research (grant 12-02-00208).

References

[1] J. Coey, M. Viret, S. Molnar, Adv. Phys. 48 (1999) 167–293.
[2] M.B. Salamon, M. Jaime, Rev. Mod. Phys. 73 (2001) 583–628.
[3] P.K. Siwach, H.K. Singh, O.N. Srivastava, J. Phys.: Condens. Matter 20 (2008) 273201. 1–43.
[4] N.G. Bebenin, Phys. Metal. Metall. 111 (2011) 236–252.
[5] E.O. Wollan, W.C. Koehler, Phys. Rev. 100 (1955) 545–563.
[6] N.N. Loshkareva, E.V. Mostovshchikova, Phys. Metal. Metall. 113 (2012) 19–38.
[7] N.N. Loshkareva, L.V. Nomerovannaya, E.V. Mostovshchikova, A.A. Makhnev, Yu.P. Sukhorukov, N.I. Solin, T.I. Arbuzova, S.V. Naumov, N.V. Kostromitina, Phys. Rev. B 70 (2004) 224406. 1–8.
[8] K.R. Poeppelmeier, M.E. Leonowicz, J.M. Longo, Solid State Chem. 44 (1982) 89–98.
[9] A. Reller, J.M. Thomas, D.A. Jefferson, Proc. Roy. Soc. Lond. A 394 (1984) 223–241.
[10] B. Raveau, Y.M. Zhao, C. Martin, M. Hervieu, A. Maignan, J. Solid State Chem. 149 (2000) 203–207.
[11] L. Pi, S. Hebert, C. Martin, A. Maignan, B. Raveau, Phys. Rev. B 67 (2003) 024430. 1–7.
[12] C. Martin, M. Miclau, S. Hebert, M. Giot, A. Maignan, G. Andre, F. Bouree-Vigneron, JMMM 321 (2009) 3938–3944.
[13] A. Maignan, C. Martin, C. Autret, M. Hervieu, B. Raveau, J. Hejtmanek, J. Mater. Chem. 12 (2002) 1806–1811.
[14] C. Martin, A. Maignan, M. Hervieu, B. Raveau, J. Hejtmanek, Phys. Rev. B 63 (2001) 100406(R). 1–4.
[15] R. Ang, Y.P. Sun, Y.Q. Ma, B.C. Zhao, X.B. Zhu, W.H. Song, J. Appl. Phys. 100 (2006) 063902. 1–11.
[16] Li Pi, Shixiong Zhang, Wei Tong, Shun Tan, Yuheng Zhang, Solid State Commun. 139 (2006) 460–464.
[17] Y. Murano, M. Matsukawa, S. Ohuchi, S. Kobayashi, S. Nimori, R. Suryanarayanan, K. Koyama, N. Kobayashi, Phys. Rev. B 83 (2011) 054437. 1–13.
[18] H.J. McSkimin, in: W.P. Mason (Ed.), Physical Acoustics. Principles and Methods, vol. 1, Part A, Academic Press, New York, 1964, pp. 272–334.
[19] R.I. Zainullina, N.G. Bebenin, A.M. Burkhanov, V.V. Ustinov, Ya.M. Mukovskii, Phys. Rev. B 66 (2002) 064421. 1–5.
[20] R.I. Zainullina, N.G. Bebenin, A.M. Burkhanov, V.V. Ustinov, Y.M. Mukovskii, J. Alloy Comp. 394 (2005) 39–42.
[21] R.K. Zheng, C.F. Zhu, J.Q. Xie, X.G. Li, Phys. Rev. B 63 (2000) 024427. 1–4.
[22] E. Rozenberg, M. Auslender, A.I. Shames, C. Martin, S. Hebert, J. Appl. Phys. 103 (2008) 07F720. 1–3.
[23] C.M. Varma, Phys. Rev. B 54 (1996) 7328–7333.